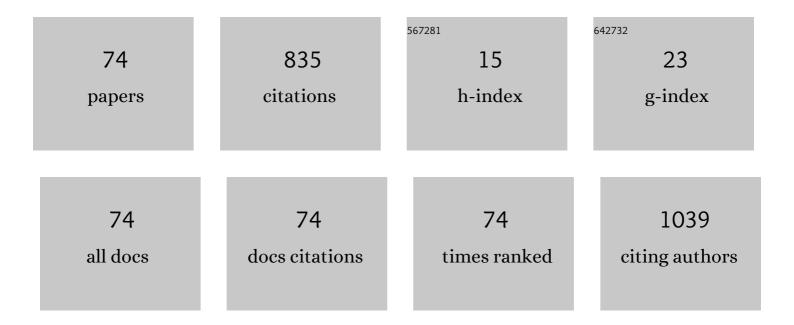
List of Publications by Year in descending order

Source: https://exaly.com/author-pdf/8909844/publications.pdf

Version: 2024-02-01



#	Article	IF	CITATIONS
1	Deep learning image reconstruction algorithm for pancreatic protocol dual-energy computed tomography: image quality and quantification of iodine concentration. European Radiology, 2022, 32, 384-394.	4.5	27
2	Arterial involvement and resectability scoring system to predict RO resection in patients with pancreatic ductal adenocarcinoma treated with neoadjuvant chemoradiation therapy. European Radiology, 2022, 32, 2470-2480.	4.5	9
3	Response prediction of neoadjuvant chemoradiation therapy in locally advanced rectal cancer using CT-based fractal dimension analysis. European Radiology, 2022, 32, 2426-2436.	4.5	3
4	Uterine extension determined by MRI: a useful parameter for differentiating subserosal leiomyomas from ovarian tumors. Abdominal Radiology, 2022, , 1.	2.1	2
5	Prognostic value of <sup>18</sup> F-FDG PET/CT and MRI features in patients with high-risk and very-high-risk cutaneous squamous cell carcinoma. British Journal of Radiology, 2022, 95, 20211003.	2.2	2
6	MRI findings of epithelial–myoepithelial carcinoma of the parotid gland with radiologic–pathologic correlation. Japanese Journal of Radiology, 2022, 40, 578-585.	2.4	4
7	Spatiotemporal imaging of redox status using in vivo dynamic nuclear polarization magnetic resonance imaging system for early monitoring of response to radiation treatment of tumor. Free Radical Biology and Medicine, 2022, 179, 170-180.	2.9	2
8	A comparative analysis of MRI findings in endometrial cancer: differentiation between endometrioid adenocarcinoma, serous carcinoma, and clear cell carcinoma. European Radiology, 2022, 32, 4128-4136.	4.5	6
9	MRI-based radiomics analysis for differentiating phyllodes tumors of the breast from fibroadenomas. European Radiology, 2022, 32, 4090-4100.	4.5	13
10	Prediction of overall survival in patients with pancreatic ductal adenocarcinoma: histogram analysis of ADC value and correlation with pathological intratumoral necrosis. BMC Medical Imaging, 2022, 22, 23.	2.7	9
11	Radiological Arterial Anatomy in Mature Microminipigs as a Pre-clinical Research Model in Interventional Radiology. CardioVascular and Interventional Radiology, 2022, , 1.	2.0	0
12	Imaging findings of malignant skin tumors: radiological–pathological correlation. Insights Into Imaging, 2022, 13, 52.	3.4	5
13	Unenhanced abdominal low-dose CT reconstructed with deep learning-based image reconstruction: image quality and anatomical structure depiction. Japanese Journal of Radiology, 2022, 40, 703-711.	2.4	10
14	Radiation and iodine dose reduced thoraco-abdomino-pelvic dual-energy CT at 40 keV reconstructed with deep learning image reconstruction. British Journal of Radiology, 2022, 95, 20211163.	2.2	10
15	Vascular involvement and resectability of pancreatic ductal adenocarcinoma on contrast-enhanced MRI: comparison with pancreatic protocol CT. Abdominal Radiology, 2022, 47, 2835-2844.	2.1	6
16	Comparison of the Diagnostic Value of Mono-exponential, Bi-exponential, and Stretched Exponential Signal Models in Diffusion-weighted MR Imaging for Differentiating Benign and Malignant Hepatic Lesions. Magnetic Resonance in Medical Sciences, 2021, 20, 69-75.	2.0	7
17	Hepatobiliary contrast uptake patterns on gadoxetic acid–enhanced MRI in liver metastases from pancreatic ductal adenocarcinoma: can it predict prognosis?. European Radiology, 2021, 31, 276-282.	4.5	2
18	Utility of texture analysis on T2-weighted MR for differentiating tumor deposits from mesorectal nodes in rectal cancer patients, in a retrospective cohort. Abdominal Radiology, 2021, 46, 459-468.	2.1	9

#	Article	IF	CITATIONS
19	Simulated twin-phase pancreatic CT generated using single portal venous phase dual-energy CT acquisition in pancreatic ductal adenocarcinoma. Abdominal Radiology, 2021, 46, 2610-2619.	2.1	5
20	Low keV portal venous phase as a surrogate for pancreatic phase in a pancreatic protocol dual-energy CT: feasibility, image quality, and lesion conspicuity. European Radiology, 2021, 31, 6898-6908.	4.5	10
21	Advantages and disadvantages of single-source dual-energy whole-body CT angiography with 50% reduced iodine dose at 40 keV reconstruction. British Journal of Radiology, 2021, 94, 20201276.	2.2	13
22	Deep learning image reconstruction for pancreatic low-dose computed tomography: comparison with hybrid iterative reconstruction. Abdominal Radiology, 2021, 46, 4238-4244.	2.1	26
23	Low-dose whole-body CT using deep learning image reconstruction: image quality and lesion detection. British Journal of Radiology, 2021, 94, 20201329.	2.2	22
24	Development of 20Âcm sample bore size dynamic nuclear polarization (DNP)-MRI at 16ÂmT and redox metabolic imaging of acute hepatitis rat model. Free Radical Biology and Medicine, 2021, 169, 149-157.	2.9	0
25	Optimized scan delay for late hepatic arterial or pancreatic parenchymal phase in dynamic contrast-enhanced computed tomography with bolus-tracking method. British Journal of Radiology, 2021, 94, 20210315.	2.2	3
26	In Vivo Dynamic Nuclear Polarization Magnetic Resonance Imaging for the Evaluation of Redox-Related Diseases and Theranostics. Antioxidants and Redox Signaling, 2021, , .	5.4	3
27	CT and MRI characteristics of ovarian mature teratoma in patients with anti-N-methyl-D-aspartate receptor encephalitis. Diagnostic and Interventional Imaging, 2021, 102, 447-453.	3.2	4
28	Effect of computed tomography value error on dose calculation in adaptive radiotherapy with Elekta Xâ€ray volume imaging cone beam computed tomography. Journal of Applied Clinical Medical Physics, 2021, 22, 271-279.	1.9	2
29	Comparison of mono-exponential, bi-exponential, and stretched exponential diffusion-weighted MR imaging models in differentiating hepatic hemangiomas from liver metastases. European Journal of Radiology, 2021, 141, 109806.	2.6	6
30	Optimized Bolus Threshold for Dual-Energy CT Angiography with Monoenergetic Images: A Randomized Clinical Trial. Radiology, 2021, 300, 615-623.	7.3	5
31	Diffusion-weighted imaging of the abdomen using echo planar imaging with compressed SENSE: Feasibility, image quality, and ADC value evaluation. European Journal of Radiology, 2021, 142, 109889.	2.6	13
32	Utility of Noncontrast Magnetic Resonance Angiography for Aneurysm Follow-Up and Detection of Endoleaks after Endovascular Aortic Repair. Korean Journal of Radiology, 2021, 22, 513.	3.4	7
33	Hepatocyte fraction: correlation with noninvasive liver functional biomarkers. Abdominal Radiology, 2020, 45, 83-89.	2.1	7
34	Pancreatic extracellular volume fraction using T1 mapping in patients with impaired glucose intolerance. Abdominal Radiology, 2020, 45, 449-456.	2.1	11
35	lodine dose optimization in portal venous phase virtual monochromatic images of the abdomen: Prospective study on rapid kVp switching dual energy CT. European Journal of Radiology, 2020, 122, 108746.	2.6	14
36	Utility of microcatheter in adrenal venous sampling for primary aldosteronism. British Journal of Radiology, 2020, 93, 20190636.	2.2	10

#	Article	IF	CITATIONS
37	Detection of pancreatic ductal adenocarcinoma and liver metastases: comparison of Gd-EOB-DTPA-enhanced MR imaging vs. extracellular contrast materials. Abdominal Radiology, 2020, 45, 2459-2468.	2.1	6
38	Magnetic resonance cholangiopancreatography using optimized integrated combination with parallel imaging and compressed sensing technique. Abdominal Radiology, 2019, 44, 1766-1772.	2.1	11
39	Prognostic evaluation of pancreatic ductal adenocarcinoma: Associations between molecular biomarkers and CT imaging findings. Pancreatology, 2019, 19, 331-339.	1.1	5
40	The feasibility of dedicated breast PET for the assessment of residual tumor after neoadjuvant chemotherapy. Japanese Journal of Radiology, 2019, 37, 81-87.	2.4	9
41	Gadoxetic acid-enhanced dynamic magnetic resonance imaging using optimized integrated combination of compressed sensing and parallel imaging technique. Magnetic Resonance Imaging, 2019, 57, 111-117.	1.8	19
42	Correlation of quantitative pancreatic T <sub>1</sub> value and HbA1c value in subjects with normal and impaired glucose tolerance. Journal of Magnetic Resonance Imaging, 2019, 49, 711-718.	3.4	12
43	Thin-slice Free-breathing Pseudo-golden-angle Radial Stack-of-stars with Gating and Tracking T <sub>1</sub> -weighted Acquisition: An Efficient Gadoxetic Acid-enhanced Hepatobiliary-phase Imaging Alternative for Patients with Unstable Breath Holding. Magnetic Resonance in Medical Sciences, 2019, 18. 4-11.	2.0	13
44	Modified National Comprehensive Cancer Network Criteria for Assessing Resectability of Pancreatic Ductal Adenocarcinoma. American Journal of Roentgenology, 2018, 210, 1252-1258.	2.2	15
45	Utility of the portal venous phase for diagnosing pancreatic necrosis in acute pancreatitis using the CT severity index. Abdominal Radiology, 2018, 43, 3035-3042.	2.1	3
46	Simultaneous acquisition of MR angiography and diagnostic images of abdomen at viewâ€sharing multiarterial phases and comparing the effect of two different contrast agents. Journal of Magnetic Resonance Imaging, 2018, 48, 102-110.	3.4	2
47	Optimal window settings in single-source dual-energy computed tomography of the abdomen. European Journal of Radiology, 2018, 109, 204-209.	2.6	17
48	Assessing Chemotherapeutic Response in Pancreatic Ductal Adenocarcinoma: Histogram Analysis of Iodine Concentration and CT Number in Single-Source Dual-Energy CT. American Journal of Roentgenology, 2018, 211, 1221-1226.	2.2	26
49	Prognostic Value of Diffusion MR Imaging and Clinical-Pathologic Factors in Patients with Rectal Cancer. Iranian Journal of Radiology, 2018, 15, .	0.2	5
50	Visualization of right adrenal vein: Comparison with three phase dynamic contrast-enhanced CT. European Journal of Radiology, 2017, 96, 104-108.	2.6	3
51	Additional value of venous phase added to aortic CT angiography in patients with aortic aneurysm. Clinical Imaging, 2017, 44, 51-56.	1.5	2
52	Improved diagnosis of common bile duct stone with single-shot balanced turbo field-echo sequence in MRCP. Abdominal Radiology, 2017, 42, 1183-1188.	2.1	5
53	Gadoxetic acid-enhanced high temporal-resolution hepatic arterial-phase imaging with view-sharing technique: Impact on the LI-RADS category. European Journal of Radiology, 2017, 94, 167-173.	2.6	7
54	Transcatheter Arterial Embolization for Primary Postpartum Hemorrhage: Predictive Factors of Need for Embolic Material Conversion of Gelatin Sponge Particles to N-Butyl Cyanoacrylate. CardioVascular and Interventional Radiology, 2017, 40, 236-244.	2.0	11

#	Article	IF	CITATIONS
55	Findings in pancreatic MRI associated with pancreatic fibrosis and HbA1c values. Journal of Magnetic Resonance Imaging, 2016, 43, 680-687.	3.4	23
56	Diffusion kurtosis imaging of the pancreas for the assessment of HbA1c levels. Journal of Magnetic Resonance Imaging, 2016, 43, 159-165.	3.4	13
57	Biliary tract enhancement in gadoxetic acid-enhanced MRI correlates with liver function biomarkers. European Journal of Radiology, 2016, 85, 2001-2007.	2.6	11
58	F-18 FDG uptake on positron emission tomography as a predictor for lymphovascular invasion in patients with lung adenocarcinoma. Annals of Nuclear Medicine, 2016, 30, 11-17.	2.2	15
59	Determination of the least amount of iodine load required for the detection of pancreatic adenocarcinoma at 80-kVp CT. European Journal of Radiology, 2016, 85, 901-905.	2.6	7
60	Minimally Required Iodine Dose for the Detection of Hypervascular Hepatocellular Carcinoma on 80-kVp CT. American Journal of Roentgenology, 2016, 206, 518-525.	2.2	14
61	Multiphase Contrast-Enhanced Magnetic Resonance Imaging Features of Bacillus Calmette-Guérin-Induced Granulomatous Prostatitis in Five Patients. Korean Journal of Radiology, 2015, 16, 342.	3.4	20
62	MRI of the Thyroid for Differential Diagnosis of Benign Thyroid Nodules and Papillary Carcinomas. American Journal of Roentgenology, 2015, 204, W332-W335.	2.2	45
63	Low-Iodine-Load and Low-Tube-Voltage CT Angiographic Imaging of the Kidney by Using Bolus Tracking with Saline Flushing. Radiology, 2015, 275, 832-840.	7.3	30
64	Whole-body CT with high heat-capacity X-ray tube and automated tube current modulation—Effect of tube current limitation on contrast enhancement, image quality and radiation dose. European Journal of Radiology, 2015, 84, 877-883.	2.6	5
65	18-F fluorodeoxyglucose uptake in positron emission tomography as a pathological grade predictor for renal clear cell carcinomas. European Radiology, 2015, 25, 3009-3016.	4.5	25
66	Computer-aided assessment of hepatic contour abnormalities as an imaging biomarker for the prediction of hepatocellular carcinoma development in patients with chronic hepatitis C. European Journal of Radiology, 2015, 84, 811-815.	2.6	4
67	Reducing iodine load in hepatic CT for patients with chronic liver disease with a combination of low-tube-voltage and adaptive statistical iterative reconstruction. European Journal of Radiology, 2015, 84, 11-18.	2.6	35
68	Prediction of early response to uterine artery embolization in fibroids: Value of MR signal intensity ratio. Magnetic Resonance Imaging, 2015, 33, 51-55.	1.8	10
69	Prenatal MR imaging diagnosis of placental invasion. Abdominal Imaging, 2015, 40, 1273-1278.	2.0	15
70	Characterizing focal hepatic lesions by free-breathing intravoxel incoherent motion MRI at 3.0 T. Acta Radiologica, 2014, 55, 1166-1173.	1.1	33
71	Peritoneal chronic inflammatory mass formation due to gallstones lost during laparoscopic cholecystectomy. Clinical Imaging, 2014, 38, 758-761.	1.5	4
72	Whole-Body CT Angiography With Low Tube Voltage and Low-Concentration Contrast Material to Reduce Radiation Dose and Iodine Load. American Journal of Roentgenology, 2014, 202, W106-W116.	2.2	47

#	Article	IF	CITATIONS
73	Whole-body CT screening: scan delay and contrast injection duration for optimal enhancement of abdominal organs and deep vessels. Clinical Imaging, 2014, 38, 129-135.	1.5	1
74	Reduction of Iodine Load in CT Imaging of Pancreas Acquired With Low Tube Voltage and an Adaptive Statistical Iterative Reconstruction Technique. Journal of Computer Assisted Tomography, 2014, 38, 714-720.	0.9	20